An agarose disk electroporation method for *ex vivo* retinal tissue cultured at the air-liquid interface reveals electrical stimulus-induced cell cycle reentry in retinal cells

Megan L. Stone[1], Hannah H. Lee[2] , Edward M. Levine[1,2,*]

[1]Department of Cell and Developmental Biology
Vanderbilt University, Nashville TN 37232

[2]Department of Ophthalmology and Visual Sciences
Vanderbilt University Medical Center, Nashville TN 37232

*Corresponding author
Ed.levine@vumc.org

Funding was generously provided by a Ruth L. Kirschstein Predoctoral Individual National Research Service Award (F31EY035554) (MLS), Janet and Jim Ayers Research Fund in Regenerative Visual Science (EML), the William A. Black Chair in Ophthalmology (EML), and through an unrestricted grant from Research to Prevent Blindness, Inc. to the Department of Ophthalmology and Visual Sciences.

Keywords:

Ethics statement: All procedures and experiments with mice were approved under protocol M1600035 by the Vanderbilt Institutional Animal Care and Use Committee and conformed to the ARVO guidelines for the use of animals in vision research. The research was conducted in concordance with the NIH guidelines for Responsible Conduct in Research (RCR).

The authors declare no conflicts of interest

Motivation

Tissues cultured at the air-liquid interface, such as retinal tissue, are adhered to a filter membrane with media underneath but not fully submerged. If tissues are fully submerged in liquid, they detach from the membrane and become damaged. Electroporation typically requires tissue submergence for electric current flow. We have developed a submergence-free electroporation method using an agarose disk for electric current delivery that can efficiently and consistently electroporate *ex vivo* retinal tissue cultured at an air-liquid interface without the need to submerge the tissue and disrupt the culture system.

Summary

It is advantageous to culture the *ex vivo* murine retina along with many other tissue types at the air-liquid interface. However, gene delivery to these cultures can be challenging. Electroporation is a fast and robust method of gene delivery, but typically requires submergence in a liquid buffer to allow electric current flow. We have developed a submergence-free electroporation technique using that allows for efficient gene delivery to the *ex vivo* murine retina. This method advances our ability to use *ex vivo* retinal tissue for genetic studies and can easily be adapted for any tissue cultured at an air-liquid interface. Use of this method has revealed valuable insights on the state of *ex vivo* retinal tissues and the effects of electrical stimulation on retinal cells.

Introduction

The retina is a highly structured organ that relies on intercellular communication to respond to injury and maintain homeostasis[1–3]. The field of retinal research relies on various model systems to study the structure, function, and pathology of the retina. *Ex vivo* explant systems involve isolating and culturing tissue samples, which allows for the preservation of the complex structure and physiological characteristics of organs like the retina[4–6]. *Ex vivo* retinal tissue cultures offer several advantages over other models, particularly in the study of retinal function and degeneration. *Ex vivo* models allow the study of cellular changes within the context of the tissue structure compared to *in vitro,* which lack the 3-dimensional context, or organoid models, which lack prior organismal physiological integration and external environmental exposures. Furthermore, *ex vivo* models provide the opportunity for more advanced manipulations and analyses that may be difficult to perform and interpret *in vivo*, such as live imaging, small molecule delivery and cell reprogramming studies[7,8].

Ex vivo retinal tissues experience cell death and activation of Müller glia over time in culture. This makes *ex vivo* retinal explant models particularly valuable as an injury model[6,9–12]. It is of interest to improve the health of these cultures to study the retina under normal physiological conditions, however. Innovations in culture technique and supplementation has been shown to promote the survival of *ex vivo* retinal explants. One such innovation is to culture tissue on PTFE membrane inserts with media below the membrane filter. This technique maintains an air-liquid interface that is valuable for gas exchange in the tissue[9,13,14]. Optimization studies to preserve the health of *ex vivo* tissues are ongoing, but as is, long term culture of *ex vivo* retinal tissue is a useful injury context to observe live changes in response to genetic manipulation.

Gene delivery to *ex vivo* retinal tissue can be challenging. Viral methods, such as AAV and lentivirus, are limited by size constraints for DNA cargo and have delayed expression time compared to non-viral methods[15,16]. Electroporation is a robust method for plasmid delivery that promotes quick expression. However, electroporation requires that cells or tissues be submerged in buffer with an electrode to allow electric current flow. Submersion of tissue is feasible prior to culture, but submerging tissues at the air-liquid interface causes detachment from the support membrane, which restricts the ability to transfect after cultures are established.

To overcome the obstacles to delivery of genetic material to *ex vivo* retinal tissues, we developed an electroporation method that avoids tissue submergence in a large volume by generating a confined liquid interface between the electrode and sample (Figure 1). With this adaptation, we characterized the efficiency of electroporation at 1- and 14-days *ex vivo* (DEV) in the air-liquid interface culture format. We also characterized the effects of electrical stimulation on cell proliferation in *ex vivo* retinal cultures. Lastly, we investigate the limitations in assessing transfection efficiency when relying on a fluorescent reporter construct as a readout.

Results

Agarose disk electroporation of *ex vivo* retinal tissue efficiently delivers genetic material with minimal tissue submergence

The components required for this electroporation system are: (1) an arm electrode that can be fixed to a ring stand and lowered onto cultured tissues in cell culture insert, (2) a 0.5% agarose disk, 5mm thick and the width of the arm electrode, (3) DNA with an electroporation dye containing glycerol to increase viscosity, and (4) an

anode dish underneath the tissue to complete the electrical circuit. Electroporation was performed at 24 hours (1DEV) or 14 days (14DEV). All *ex vivo* retinal explant tissues were dissected from mice between 8-12 weeks of age.

To create a complete electric circuit, chilled PBS (4°C) is placed on the anode surface and the cell culture insert containing the retinal tissue is placed on top (Figure 1A, B). A 0.5% agarose disk roughly 10mm wide is adhered to the arm electrode surface (Figure 1C). The disk should be adhered with no air bubbles formed between it and the electrode, which could impede electrical flow. Once the agarose disk is adhered to the electrode, 10-15uL of DNA-glycerol mixture (1-3 pMol DNA, 2.5% methyl green dye and 7.5% glycerol) is pipetted on top of the agarose disk facing upward (Figure 1C, D). The electrode is rotated 180 degrees and the DNA mixture will stay adhered to the agarose as a suspended drop. The arm electrode is lowered until the DNA mixture contacts the tissue, at which point current is delivered (Figure 1E). Fluorescent reporter-expressing plasmids with a general promoter, such as pCMV-eGFP, were used to assess transfection.

Differences in cell types transfected at the edge and center of the tissue at 1DEV

Since tissues were cultured with their basal surface toward the air-liquid interface, the cells most accessible to plasmid uptake were astrocytes, retinal ganglion cells, displaced amacrine cells, and Müller glia[17,18]. Electroporation of pCMV-eGFP at 1DEV revealed a consistent difference in morphology from cells transfected at the center of the retina compared to the edge that is defined as 100µm in from tissue periphery around perimeter (Figure 2B). Cells transfected at the edge of the tissue

resembled Müller glia in morphology (Figure 2D, G). Colocalization of eGFP with SOX9, a marker of Müller glia[19–21], is consistent with this observation (Figure 2D). In contrast, transfected cells toward the center of the tissue had a retinal ganglion cell-like morphology, which is distinctly recognizable by long axons converging at the optic nerve head (Figure 2C, F). Electroporation of pCMV-mCherry into retinas from Thy1:YFP-16 mice (Thy1:YFP), which express YFP in a large cohort of RGCs in addition to other inner retinal neurons[22], provided further evidence that RGCs were transfected (Figure 2G). Quantifications revealed that the distributions of transfected cells were skewed toward SOX9+ cells at the tissue edge and toward Thy1:YFP+ cells toward the center (Figure 2H). Overall, there is equivalent efficiency in transfection of Müller glia and Thy1:YFP+ cells at 1DEV, but their distribution is location-dependent (Figure 2H).

Müller glia are preferentially transfected at 14DEV

Changes in cell survival, location, size, and morphology occur over time in culture[10–12]. Retinal tissue was electroporated at 14DEV to assess differences in transfection profile over time. Cells transfected at the edge of tissue resembled Müller glial morphology (Figure 3D, G), but the characteristic retinal ganglion cell morphology visible in the center at 1DEV was not observed (Figure 3C, D, F, G). Staining for SOX9 revealed an increase in transfected Müller glia compared to inner retinal neurons as assessed with Thy1:YFP regardless of location (Figure 3D, G). These observations suggest that there is a decrease in neurons transfected at 14DEV overall, and an increase in transfection of Müller glia at the tissue center (Figure 3H).

To visualize tissue structure with respect to inner neurons and Müller glia at 1 and 14DEV, orthogonal slice projections were constructed from Z-stack confocal images of Thy1:YFP or Rlbp1:GFP transgenic retinas, the latter serving as a reporter for Müller glia[23]. An ROI "slice" was cropped from each image in the same orientation to observe center and edge regions (Figure 4). At 1DEV, YFP+ cells were observed in the ganglion cell layer and inner nuclear layer (Figure 4A). Also observed was a line of fluorescence in the inner plexiform layer, suggesting maintained laminar organization. However, fewer YFP+ cells were observed in the ganglion cell layer at the retinal edge (Figure 4A, left). At 14DEV, YFP expression in the ganglion cell layer was diminished in the central region but interestingly was retained in the inner plexiform and nuclear layers (Figure 4B). In Rlbp1:GFP tissue, GFP expression was also detectable at the ganglion cell surface in the center of tissue at 1DEV (Figure 4C), consistent with their radial morphology[24]. At 14DEV, there was an increase in GFP expression throughout the tissue including at the electroporation surface (Figure 4D), most likely the result of the extended time in culture. The loss of RGCs and accumulation of Müller glia at the basal surface of the tissue could explain the shift toward preferential electroporation of Müller glia at 14DEV.

Electrical stimulation induces BrdU incorporation in *ex vivo* retina

The adult mouse retina is normally quiescent, but proliferation can occur to a limited extent in non-neuronal cells such as microglia and Müller glia in response to injury and/or inflammation, two contexts that are likely occurring in the *ex vivo* retina [6,10,12,25–30]. Proliferation has also been shown to increase in response to electrical

stimulation[31–35], though this has yet to be shown in the retina. We therefore assessed proliferation in the cultures with and without electroporation to obtain baseline measurements. Three conditions were tested: not electroporated (-*EP*), electroporated with DNA loading solution but lacking DNA (+*EP*), or electroporated with pCMV-eGFP plasmid (+EP^{DNA}). These treatments were applied to *ex vivo* retinas at 1DEV or 14DEV. At 72 hours post-treatment,16uM BrdU was delivered in the cell culture media for 24 hours (Figure 5A). At both times in culture, there were significant increases in BrdU+ cells per mm^3 in the +*EP* and +EP^{DNA} conditions compared to the -*EP* condition (Figure 5B,C). The similar levels of BrdU incorporation in the +*EP* and +EP^{DNA} conditions were expected since eGFP was being expressed. These results indicate that electrical pulse application is sufficient to promote proliferation in *ex vivo* retinal tissue.

The proportion of BrdU+ cells that are Müller glia increases in 14DEV compared to 1DEV cultures and following electrical stimulus

We predicted that microglia and Müller glia were re-entering the cell cycle in response to electrical stimulation. To assess this, *ex vivo* retinal tissues were immunostained with the microglial marker IBA1 or with SOX9 in combination with BrdU detection, and colocalization with BrdU was quantified to determine the number of these cells undergoing cell cycle entry (Figure 6). At 1 and 14DEV, BrdU+ microglia and Müller glia were observed in -*EP* and +*EP* conditions (Figure 6A, B). Quantification revealed a significantly increased proportion of BrdU+ Müller glia, indicated by SOX9 labeling, at 14DEV in +*EP* tissues compared to 1DEV +*EP* (Figure 6C). The number of BrdU+ Müller glia significantly increased in +*EP* tissues at 14DEV compared to 1DEV

+*EP* tissues and 14DEV -*EP* tissues, whereas the number of BrdU+ microglia remained steady (Figure 6D). These results suggest an increase in cell cycle entry in Müller glia that correlates with time in culture and electrical stimulation.

Transfection efficiency is greater than what is observable through fluorescent protein expression when delivering a fluorescent reporter construct

A limitation of using fluorescent reporter expression constructs such as pCMV-eGFP is that cells could have been transfected but expression of the fluorescent protein was below detection. Since as few as 4 molecules of Cre recombinase are sufficient for recombination[36–38], we predicted that transfection of a Cre expression construct into a mouse harboring a recombination reporter allele would reveal a higher transfection efficiency than what can be detected with pCMV-eGFP (Figure 7A). To test this, pCMV-Cre and pCMV-eGFP were co-transfected at equimolar concentrations into *ex vivo* retinal tissues from mice with a Cre-inducible *Rosa*^{Al14} allele. *Ex vivo* tissues were imaged every 24 hours and fixed at 72 hours post-electroporation.

In cultures transfected at 1DEV (Figure 7B) or 14DEV (Figure 7C), similar trends were observed at the tissue center and edge. Whereas the majority of eGFP+ cells were tdTomato (tdTom)+, many tdTom+ cells were not eGFP+ (Venn diagrams in Figure 7B,C). Quantifications revealed a significant increase in the number of co-labeled cells per the eGFP population compared to the tdTom population at both timepoints (Figure 7D). The transfection efficiency and level of expression of these constructs is expected to be similar based on the promoter elements shared between them.

Additionally, there were significant increases in the percentages of all transfected cells expressing tdTom compared to eGFP in the 1DEV and 14DEV cultures (Figure 7E). These data suggest that the transfection efficiency is greater than what can be observed by transfection of expression plasmids for fluorescent proteins.

Discussion

This study introduces an agarose disk submergence-free method of electroporation for *ex vivo* retinal tissue cultured at the air-liquid interface. This electroporation method offers a rapid and time-dependent transfection efficiency while maintaining tissue integrity. This method is cost effective and does not require specialized equipment, making it generally accessible. Though we have only tested retinal tissue, it could easily be adapted for any tissue type that is cultured using an air liquid interface method, including lung, intestine, or skin[13,14,39,40].

We observed a significant difference in the cell types transfected at different times in culture. This finding suggests that the timing of the transfection is useful for targeting specific cell populations within the retina. Müller glia undergo hypertrophy and migration in response to injury signals from retinal neurons[41–45]. Likely, the increase in availability of Müller glia at the electroporation surface is due to the loss of retinal ganglion cells and changes in Müller glial morphology associated with tissue remodeling[46].

We found that the application of electrical stimulus alone leads to an increase in proliferation in Müller glia as indicated by BrdU incorporation. The mammalian retina is quiescent after retinal development, but Müller glia and microglia are known to exhibit

limited proliferation in response to injury or inflammation. This proliferation occurs typically in young postmitotic mice and diminishes after injury onset[6,10,12,25–27,30,42,45]. Postmitotic Müller glia have been shown to proliferate in culture, however this effect was observed in *ex vivo* retinal tissues from P10 mice and diminished by p14[10]. The mice used here were adults between 8-12 weeks of age. This indicates a change in cell behavior following electrical stimulus that is not typical under normal physiological conditions.

Proliferation resulting from electrical stimulation has been reported in multiple cell types, including neural stem cells, human embryonic stem cells, osteoblasts, and fibroblasts[31,47–50]. Electroporation can also stimulate neural progenitor cells differentiate into neurons[50–52]. Amongst the BrdU+ cell population, there was a significant increase in BrdU+ Müller glia at later timepoints and following electrical stimulus whereas the presence of BrdU+ microglia was not dependent on time in culture. This could indicate an increase in Müller glia in the tissue at this timepoint or a change in cell state that leads to increased proliferation of Müller glia. Further studies are needed to determine whether proliferating Müller glia in this context also acquire neurogenic properties.

Lastly, deliver of a Cre expression construct into a recombination reporter mouse strain predicts that that true transfection efficiency is greater than observed with a fluorescent reporter expression construct, meaning more cells may receive gene delivery than accounted for. It is advantageous with this system to use a sensitive reporter for electroporation, like Cre-mediated reporter expression, or to boost the signal for the fluorescent reporter with antibodies to enhance detection.

Limitations of Study

While this study provides valuable insights into the overall efficiency of transfection, especially on some retinal cell types, further research is necessary to fully characterize the effects on every cell type. This method has only been tested on retinal tissue, though it could be adapted for other tissue types cultured in an air-liquid interface format. Proliferation observed in this study was measured using BrdU incorporation, which labeled cells during S-phase of mitosis. BrdU could incorporate in cells that are then arrested in S-phase and do not fully divide. Further testing is required to understand the extent of proliferation following electrical stimulation.

Although certain cell types may be more amenable to electroporation, the method is not inherently cell type specific. Other methods of transfection should be employed if a study requires expression to only occur in certain cell types. We demonstrated that BrdU incorporation is induced following electrical stimulation with this method. If a study is designed to test the effects of an electroporated construct on proliferation, an important control would be the inclusion of an *EP* condition without DNA in addition to the negative control plasmid.

Acknowledgments

E.M.L received funding from M.L.S was supported by Janet and Jim Ayers Research Fund in Regenerative Visual Science (EML), the William A. Black Chair in Ophthalmology, and through an unrestricted grant from Research to Prevent Blindness, Inc. to the Department of Ophthalmology and Visual Sciences. M.L.S was supported by a Ruth L. Kirschstein Predoctoral Individual National Research Service Award through the National Eye Institute (F31EY035554).

Author Contributions

Conceptualization, E.M.L and M.L.S; Methodology E.M.L, H.H.L, and M.L.S; Formal Analysis, M.L.S; Investigation, M.L.S, Resources, E.M.L, Data Curation, M.L.S, Writing - Original Draft - M.L.S, Writing - Review & Editing, E.M.L and M.L.S, Visualization, M.L.S, Supervision, E.M.L, Project Administration, E.M.L, Funding Acquisition, E.M.L.

Declaration of Interests

The authors declare no competing interests.

Figure Legends

Figure 1. Visual methodology of agarose disk electroporation for *ex vivo* retinal cultures. (A) Murine retinal tissue cultured at the air-liquid interface on PFTE membrane after 5 days *ex vivo* (5 DEV) (1X, Brightfield). (B) Agarose disk electroporation set-up. 5mm high, 10mm diameter 0.5% agarose disk adhered to an arm electrode above an anode dish containing *ex vivo* retinal tissue on PTFE membrane with chilled PBS underneath. (C) 12uL of DNA-glycerol mixture is pipetted onto the agarose disk facing upward. (D) DNA-Glycerol mixture on top of agarose disk facing upward. (E) 180° rotation electrode arm containing agarose disk and DNA-glycerol mixture lowered onto *ex vivo* retinal tissue.

Figure 2. Preferential transfection at 1DEV of Müller glia and neurons at the edge and center of tissue, respectively. (A) Timeline of experimental design for 1DEV transfection of wild type tissue with pCMV-eGFP reporter plasmin and staining for SOX9 to detect Müller glia. (B) Schematic indicating edge (100µm from the retina periphery) and center of tissue. (C) pCMV-eGFP transfected cells in wild-type tissue transfected at 1DEV. Scale bar: Left, 200µm. Right, 50µm. (D) Left: pCMV-eGFP transfected cells,

middle: SOX9 staining, and right: overlap of eGFP and SOX9 at the center (top) and edge (bottom) of tissue at 1DEV. Arrows indicate double-labeled cells. Scale Bar: 50µm.(E) Timeline of experimental design for 1DEV transfection of Thy1:YFP neuronal reporter tissue with pCMV-mCherry reporter plasmid. (F) pCMV-mCherry transfected cells in Thy1:YFP tissue transfected at 1DEV (YFP not shown). Scale bar: Left, 200µm, Right, 50µm. (G) Left: pCMV-mCherry transfected cells, middle: Thy1:YFP reporter, and right: overlap of mCherry and YFP at the center (top) and edge (bottom) of tissue after electroporation at 1DEV. Arrows indicate double-labeled cells. Scale Bar: 50µm. (H) Quantification of percentage of cells transfected with pCMV-eGFP that are SOX9+ and cells transfected with pCMV-mCherry that are Thy1:YFP+ at the edge, center and combined edge and center of tissue after electroporation at 1DEV. Mean ± SEM is shown. N=4-6. *$p < 0.05$, **$p < 0.01$, ***$p < 0.001$, ****$p < 0.0001$. No bracket indicates $p > 0.05$. All statistical tests performed on arcsine transformed values.

Figure 3. Preferential transfection of Müller glia at 14DEV. (A) Timeline of experimental design for 14DEV transfection of wild type tissue with pCMV-eGFP reporter plasmin and staining for SOX9 to detect Müller glia. (B) Schematic indicating edge (100µm from the retina periphery) and center of tissue. (C) pCMV-eGFP transfected cells in wild-type tissue transfected at 14DEV. Scale bar: Left, 200µm. Right, 50µm.(D) Left: pCMV-eGFP transfected cells, middle: SOX9 staining, and right: overlap of eGFP and SOX9 at the center (top) and edge (bottom) of tissue at 14DEV. Arrows indicate double-labeled cells. Scale Bar: 50µm. (E) Timeline of experimental design for 14DEV transfection of Thy1:YFP neuronal reporter tissue with pCMV-mCherry reporter

plasmid. (F) pCMV-mCherry transfected cells in Thy1:YFP tissue transfected at 14DEV (YFP not shown). Scale bar: Left 200µm, Right, 50µm. (G) Left: pCMV-mCherry transfected cells, middle: Thy1:YFP reporter, and right: overlap of mCherry and YFP at the center (top) and edge (bottom) of tissue after electroporation at 14DEV. Arrows indicate double-labeled cells. Scale Bar: 50µm. (H) Quantification of percentage of cells transfected with pCMV-eGFP that are SOX9+ and cells transfected with pCMV-mCherry that are Thy1:YFP+ at the edge, center and combined edge and center of tissue after electroporation at 14DEV. Mean ± SEM is shown. N=4-5. *$p < 0.05$, **$p < 0.01$, ***$p < 0.001$, ****$p < 0.0001$. No bracket indicates $p > 0.05$. All statistical tests performed on arcsine transformed values.

Figure 4. Changes in tissue structure at electroporation surface in orthogonal slice projections of 1DEV & 14DEV Thy:YFP and Rlbp1:GFP tissues favor electroporation of Müller glia at 14DEV. Orthogonal slice projections of center and edge created from 3D projections of ROIs (354.25 pixels by 11.76 pixels) to visualize cross sections within *ex vivo* retinal tissue from transgenic mouse models,.ONL: Outer nuclear layer. INL: Inner nuclear layer. GCL: Ganglion cell layer. IPL: Inner plexiform layer. (*) ONH: optic nerve head. (A) Orthogonal slice projections of the edge (left) and center (right) of Thy1:YFP *ex vivo* tissue fixed at 1DEV. Scale Bar:100µm. (N=4). (B) Orthogonal slice projections of the edge (left) and center (right) of Thy1:YFP *ex vivo* tissue fixed at 14DEV. (N=4). (C) Orthogonal slice projections of the edge (left) and center (right) of Rlbp1:GFP *ex vivo* tissue fixed at 1DEV. (N=4) (D) Orthogonal slice

projections of the edge (left) and center (right) of Rlbp1:GFP *ex vivo* tissue fixed at 14DEV. (N=4).

Figure 5. BrdU incorporation increases with electrical stimulation in the *ex vivo* retina. (A) Timeline of experimental design for tissue electroporated at 1 and 14DEV. BrdU is delivered in culture medium for 24 hours. Following fixation, pieces of retinal tissue were cut, stained for BrdU incorporation, and imaged using confocal microscopy. No Electroporation (-*EP*) tissues were given BrdU and fixed at the same timepoints indicated for electroporated tissues (+*EP*, +EP^{DNA}). (B) BrdU incorporation -*EP* (left), +*EP* (center) and +EP^{DNA} (right) tissues at 1DEV (top) and 14DEV (bottom). Scale Bar: 100µm. (C) Quantification of the number of BrdU+ cells detected per tissue volume (mm^3). Mean ± SEM is shown. N=5-10. *$p < 0.05$, **$p < 0.01$, ***$p < 0.001$, ****$p < 0.0001$. No bracket indicates $p > 0.05$. All statistical tests performed on arcsine transformed values.

Figure 6. Increase in BrdU+ Müller glia at 14DEV vs. 1DEV and following electrical stimulus. (A) Left: 1DEV -*EP* tissues stained for IBA1 (top left) or SOX9 (bottom left) and BrdU (top middle & bottom middle). Overlap of IBA1 & BrdU (top right) or SOX9 & BrdU (bottom right). Arrows indicate double labeled cells. Scale bar: 50µm. Right: 1DEV +*EP* tissues stained for IBA1 (top left) or SOX9 (bottom left) and BrdU (top middle & bottom middle). Overlap of IBA1 & BrdU (top right) or SOX9 & BrdU (bottom right). Arrows indicate double labeled cells. Scale bar: 50µm. (B) Left: 14DEV -*EP* tissues stained for IBA1 (top left) or SOX9 (bottom left) and BrdU (top middle & bottom middle).

Overlap of IBA1 & BrdU (top right) or SOX9 & BrdU (bottom right). Arrows indicate double labeled cells. Scale bar: 50µm. Right: 14DEV +*EP* tissues stained for IBA1 (top left) or SOX9 (bottom left) and BrdU (top middle & bottom middle). Overlap of IBA1 & BrdU (top right) or SOX9 & BrdU (bottom right). Arrows indicate double labeled cells. Scale bar: 50µm. (C)Left: Quantification of the percent of BrdU+ cells that are IBA1+ in -*EP* and +*EP* conditions at 1DEV and 14DEV. Mean ± SEM is shown. No bracket indicates $p > 0.05$. All statistical tests performed on arcsine transformed values. Right: Quantification of the percent of BrdU+ cells that are SOX9+ in -*EP* and +*EP* conditions at 1DEV and 14DEV. Mean ± SEM is shown. N=4-5. *$p < 0.05$. No bracket indicates $p > 0.05$. All statistical tests performed on arcsine transformed values. (D) Left: Quantification of colocalized SOX9+, BrdU+ cells per tissue volume (mm^3) in -*EP* and +*EP* conditions at 1DEV and 14DEV. Mean ± SEM is shown. N=5. No bracket indicates $p > 0.05$. All statistical tests performed on arcsine transformed values. Right: Quantification of colocalized SOX9+, BrdU+ cells per tissue volume (mm^3) -*EP* and +*EP* conditions at 1DEV and 14DEV. Mean ± SEM is shown. N=5-6. **$p < 0.01$, ***$p < 0.001$. No bracket indicates $p > 0.05$. All statistical tests performed on arcsine transformed values.

Figure 7. Transfection efficiency is greater than what is observed through expression of a fluorescent reporter construction. (A) Schematic of detection of pCMV-eGFP expression vs. pCMV-Cre expression in a $Rosa^{AI14}$ reporter tissue when few or many copies of the construct are transfected in a cell. (B) Left: Cells transfected with pCMV-CRE (left) or pCMV-eGFP (middle) and the overlap of these channels (right)

at the center (top) or edge (bottom) of tissues electroporated at 1DEV with both constructs at equal molar concentration. Scale bar: 100µm. Right: Euler plot demonstrating the number of cells detected as eGFP+. tdTom+ or double labeled at the center (top) and edge (bottom) of tissue at 1DEV. (C) Left: Cells transfected with pCMV-CRE (left) or pCMV-eGFP (middle) and the overlap of these channels (right) at the center (top) or edge (bottom) of tissues electroporated at 14DEV with both constructs at equal molar concentration. Scale bar: 100µm. Right: Euler plot demonstrating the number of cells detected as eGFP+. tdTom+ or double labeled at the center (top) and edge (bottom) of tissue at 14DEV. (D) Left: Quantification of the percent of colocalized cells detectable as transfected with pCMV-eGFP (eGFP+) and pCMV-Cre (tdTom+) within eGFP+ or tdTom+ populations at 1DEV. Mean ± SEM is shown. N=4. **$p < 0.01$. No bracket indicates $p > 0.05$. All statistical tests performed on arcsine transformed values. Right: Quantification of the percent of colocalized cells detectable as transfected with pCMV-eGFP (eGFP+) and pCMV-Cre (tdTom+) within eGFP+ or tdTom+ populations at 14DEV. Mean ± SEM is shown. N=4. *$p < 0.05$. No bracket indicates $p > 0.05$. All statistical tests performed on arcsine transformed values. (E) Left: Quantification of the percent of cells detectable as transfected with pCMV-eGFP (eGFP+) and pCMV-Cre (tdTom+) within the population of all transfected cells at 1DEV. Mean ± SEM is shown. N=4. **$p < 0.01$. No bracket indicates $p > 0.05$. All statistical tests performed on arcsine transformed values. Right: Quantification of the percent of cells detectable as transfected with pCMV-eGFP (eGFP+) and pCMV-Cre (tdTom+) within the population of all transfected cells at 14DEV. Mean ± SEM is shown. N=4. *p <

0.05. No bracket indicates $p > 0.05$. All statistical tests performed on arcsine transformed values.

STAR Methods

I. Resource Availability

Lead Contact

Further information and requests for resources and reagents should be directed to and will be fulfilled by the lead contact: Edward M. Levine, ed.levine@vumc.org

Materials Availability

This study did not generate new unique reagents.

Data and code availability

Microscopy and quantification data reported in this paper will be shared by the lead contact upon request.

II. Experimental model and participant details

Mice

B6/129 mice (Jackson Laboratory (#101043)): 8 weeks old, female.

Thy-1 YFP-16 (B6.Cg-Tg(Thy1-YFP)16Jrs/J) (Jackson Laboratory (#003709)): 8 to 12 weeks old, female and male.

Rlbp1-GFP (Tg(Rlbp1-GFP)1Eml (MGI: 6195229)): 8 to 12 weeks old, female and male. Rlbp1-CreERT2; Rosa^{Ai14} (129S6.Cg-Tg(Rlbp1-cre/ERT2)1Tfur (MGI:Pending); B6.Cg-*Gt(ROSA)26Sor*$^{tm14(CAG\text{-}tdTomato)Hze}$/J (Jackson Laboratory (#007914))), 8 to 12 weeks old, female and male.

All mice are co-housed in a 12h/12h light-dark cycle with water and food ad libitum. All transgenic mice are backcrossed to B/129 mice. All animal experiments with mice were approved under the protocol M1600235 by the Vanderbilt Institutional Animal Care and Use committee and conform to the ARVO guidelines for the use of animals in vision research. All possible efforts were made to minimize animal suffering and the number of animals used.

III. Method Details

Tamoxifen administration

To activate Cre recombination in transgenic mice, 2 doses of 200µg per gram body weight (GBW) of tamoxifen (Sigma Aldrich, T2859) were delivered in corn oil (Sigma Aldrich, C8267) via oral gavage. Mice were euthanized for tissue collection at least 5 days after tamoxifen treatment.

Retinal dissection

Prior to tissue harvest, dissection tools were sterilized with 70% ethanol and UV light for 15 minutes, and workstation was sterilized with 70% ethanol. 1X HBSS with Ca^{2+} and Mg^{2+} (Gibco, 14025) with 10mM HEPEs (Sigma Aldrich, H0887) and 1X

Antibiotics-Antimycotics (Gibco, 15240062) (referred to as HBSS hereon) was prepared and kept on ice. Mice were euthanized by CO_2 asphyxiation and cervical dislocation. Each eye was enucleated, rinsed in cold HBSS, then transferred to a fresh HBSS dish. Under a dissection scope and on a cold plate to keep tissues chilled, an incision was made in the cornea. The cornea was removed using spring scissors. The sclera, choroid and RPE were removed, and the retina and lens were transferred to a fresh HBSS dish. The lens was removed. Using spring scissors, 4 incisions were cut into retinal tissue from periphery through 25-40% of tissue toward optic nerve head, creating a flower-shaped retinal tissue that can be flattened.

Ex vivo retinal explant tissue culture

On the day of culture, plating media with supplements was prepared: NeuroCult™ Plating Media (Stem Cell Technologies, 05713), 1X SM1 neuronal supplement (Stem Cell Technologies, 05711) , 500µM L-Glutamine (Gibco, 25030149), and 100unit Penicillin/100µg Streptomycin (Pen/Strep) (ThermoFisher, 15140) (referred to as plating media hereon).

Retinal tissue was dissected as described above. A hydrophilic PTFE cell culture insert (Millicell, PICM0RG50) was prepared by pipetting 150uL of plating media onto insert membrane. Retinal tissue was mounted onto the PTFE membrane with the retinal apical surface (photoreceptor side) in juxtaposition. Tissue was placed into a 6-well plate (Corning, 353004) containing 1mL plating media and incubated at 37°C with 5% CO^2. After 48 hours, 500uL of initial plating media was replaced with BrainPhys™ Neuronal Medium (Stem Cell Technologies, 05790) containing 1X SM1 neuronal

supplement, 1X N2 Supplement-A (Stem Cell Technologies, 07152) and Pen/Strep (referred to as BrainPhys media hereon). 500µL of media was removed and replaced with fresh BrainPhys media every 48 hours for the extent of the culture.

Agarose Disk Electroporation

0.5% agarose (RPI, A20090) in 1X PBS was heated to dissolve. 500µL was pipetted into multiple wells of a 24-well plate(Corning, CLS3516) and left to solidify at room temperature for 30 minutes in a cell culture hood. An anode dish was made by lining a 100mm dish (Sigma Aldrich, Z358762) with aluminum foil, sterilized under UV light for 15 minutes, and connected to the electroporator (BTX, 45-0052) by clamping the anode cable onto the aluminum foil. Sterile, chilled PBS was pipetted onto the anode dish. Tools and workspace were sterilized with 70% ethanol. The PTFE insert containing the tissue culture was washed by gently dipping the membrane in fresh, sterile PBS. The PTFE insert was then placed on the PBS in the anode dish.

An arm electrode (Bulldog Bio, CUY700P7L) connected to the electroporator was mounted on a micromanipulator (Narishige, UMM-3C) with the electrode surface facing up. Using a plastic transfer pipet (Fisherbrand, 13-711-7M) cut above the tapered tip, an agarose disk was stamped from the solidified agarose and transferred using a spatula to the arm electrode face. The disk was gently pressed to ensure adherence without bubbles underneath.

The 12µL DNA-glycerol transfection solution was prepared using a combination of 3pMol plasmid DNA diluted in sterile PBS with 7.5% glycerol (Sigma Aldrich, C8267), and 2.5% methyl green dye (MCE, HYD0163). The DNA-Glycerol solution was pipetted

on top of the agarose disk and the arm electrode was rotated 180° while the DNA-glycerol solution and the agarose disk stayed adhered via surface tension. The arm electrode was lowered until the DNA solution was in contact with the tissue. Once there is contact between all components of the system, a closed circuit is formed.

Each tissue was electroporated with five 50V pulses for 50ms each with a 250ms break between pulses. The arm electrode was slowly raised to disconnect from the tissue, and the tissue was returned to the incubator.

The following plasmids were used in this study: pCMV-eGFP (Levine Lab), pCMV-mCherry (ClonTech, 632524), pCMV-Cre (Addgene, 123133).

Retinal explant culture tissue fixation

Culture medium was removed and replaced with room temperature PBS to wash 3 times for 10 minutes each. 100µL 1X PBS was pipetted on top of tissue for each wash. Tissues were fixed in 4% PFA for 2 hours at room temperature or at 4°C for 24 hours. PFA was removed and fixed tissues were washed 3 times with 1 mL 1X PBS for 30 minutes at room temperature. Fixed tissues were stored at 4°C in 1 mL 1X PBS with 0.01% sodium azide (Sigma Aldrich, 08591).

Whole mount immunohistochemistry

Each quadrant of the retinal tissue was separated and cut in half to generate 8 tissue fragments for staining. Individual tissue fragments were transferred into a 96-well plate (Corning, CLS3628). Tissues were washed 3 times with 1mL 1X PBS containing 1% Triton-X (1% PBST), followed by 100µL 10% normal donkey serum (NDS) (SouthernBiotech, 003001) in 1% PBST (blocking buffer) for 2 hours at room temperature. Blocking buffer was removed and tissues were stained with primary

antibodies in 1% NDS blocking buffer for 2 hours at room temperature or 24 hours at 4°C. Tissues were washed 3 times with 200µL 1% PBST for 30 minutes each. Secondary antibodies in 1% NDS blocking buffer were applied for 2 hours at room temperature. The secondary antibody was removed, and tissue was washed 3 times with 200µL 1% PBST for 30 minutes per wash. Stained tissues were mounted on Colorfrost plus slides (Fisherbrand, 12-550-17) in Fluoromount G (Invitrogen, 00-4958-02), coversliped, allowed to dry at room temperature overnight, then stored at 4°C until imaged.

The following primary antibodies were used: α-BrdU (1:200, Abcam, ab6326), α-IBA1 (1:500, FUJIFILM, 019-19741), and α-SOX9 (1:500, Chemicon, ab5535). Secondary antibodies conjugated to Alexa 488 (Invitrogen, A21206), Alexa 568 (Invitrogen, A10042), and Alexa 647 (Intvitrogen, 21247) were each diluted at 1:500.

BrdU treatment and detection

16µM BrdU was added to culture media at varying timepoints in culture per experiment. BrdU media was replenished daily until fixation. *Ex vivo* tissues were treated with BrdU for 24-72 hours depending on the experiment. Following treatment, tissues were fixed with PFA as described above. A 1/8 piece of tissue was selected at random and cut using as scalpel from the retinal culture to stain. 2N HCl (Fisher Scientific, SA541) was used for antigen retrieval for 45 minutes at room temperature, followed by a 20-minute neutralization with 0.1M sodium borate (pH 8.5) (Millipore Sigma, 1066690010). Tissues were then immunostained as described above.

Imaging

Cultures were imaged using a fluorescent stereoscope (Nikon SMZ1270i) every 48 hours post-culture establishment, and every 24 hours post-electroporation monitor for morphological, structural, or fluorescent protein expression changes within the tissue. The Zeiss LSM 710 confocal microscope was used to image tissue cultures after fixation alone or fixation and staining. Images were analyzed using FIJI version 2.9.0.

Orthogonal slice projections

To observe structural changes in *ex vivo* retinal tissue cultures, 40X Z-Stack images were obtained from the Zeiss LSM 710 confocal microscope with 1µm steps between Z slices. Using FIJI version 2.9.0, 354.25 by 11.76 pixel ROIs were selected at random but angled from tissue periphery toward optic nerve head. These ROIs were converted to 3D projections and rotated to view as a cross section.

IV. Quantification and Statistical Analysis

All cell counting and tissue volume calculations were calculated from 20X Z-stack, tile confocal images using Imaris 10.1 software. No statistical methods were used to predetermine sample sizes. GraphPad Prism 10 was used for the following statistical tests: All proportion values were arcsine transformed prior to statistical analysis. Comparisons between more than two groups were made by two-way ANOVA with Tukey post-hoc test. Comparisons between two groups within the same tissue, as in figure 7, were made using paired two-tailed t tests. Differences were considered

statistically significant at $p < 0.05$. Data are presented as mean ± SEM. Statistical significance is indicated with asterisks: *$p < 0.05$, **$p < 0.01$, ***$p < 0.001$, ****$p < 0.0001$.

References

1. Lucas RJ. Mammalian Inner Retinal Photoreception. *Curr Biol*. 2013;23(3):R125-R133. doi:10.1016/j.cub.2012.12.029

2. Vecino E, Rodriguez FD, Ruzafa N, Pereiro X, Sharma SC. Glia–neuron interactions in the mammalian retina. *Prog Retin Eye Res*. 2016;51:1-40. doi:10.1016/j.preteyeres.2015.06.003

3. Hu Y, Wang X, Hu B, et al. Dissecting the transcriptome landscape of the human fetal neural retina and retinal pigment epithelium by single-cell RNA-seq analysis. *PLoS Biol*. 2019;17(7):e3000365. doi:10.1371/journal.pbio.3000365

4. Cornwall MC, Fein A, Macnichol Jr. EM. Cellular mechanisms that underlie bleaching and background adaptation. *J Gen Physiol*. 1990;96(2):345-372.

5. Sparrow JR, Parish CA, Hashimoto M, Nakanishi K. A2E, a Lipofuscin Fluorophore, in Human Retinal Pigmented Epithelial Cells in Culture. *Invest Ophthalmol Vis Sci*. 1999;40(12):2988-2995.

6. Ueki Y, Karl MO, Sudar S, et al. P53 is required for the developmental restriction in Müller glial proliferation in mouse retina. *Glia*. 2012;60(10):1579-1589. doi:10.1002/glia.22377

7. Lee JE, Liang KJ, Fariss RN, Wong WT. Ex vivo Dynamic Imaging of Retinal Microglia using Time-lapse Confocal Microscopy. *Invest Ophthalmol Vis Sci*. 2008;49(9):4169-4176. doi:10.1167/iovs.08-2076

8. Jones MK, Lu B, Chen DZ, et al. In Vitro and In Vivo Proteomic Comparison of Human Neural Progenitor Cell-Induced Photoreceptor Survival. *PROTEOMICS*. 2019;19(3):1800213. doi:10.1002/pmic.201800213

9. Ueki Y, Reh TA. EGF stimulates müller glial proliferation via a BMP-dependent mechanism. *Glia*. 2013;61(5):778-789. doi:10.1002/glia.22472

10. Löffler K, Schäfer P, Völkner M, Holdt T, Karl MO. Age-dependent Müller glia neurogenic competence in the mouse retina. *Glia*. 2015;63(10):1809-1824. doi:10.1002/glia.22846

11. Schnichels S, Kiebler T, Hurst J, et al. Retinal Organ Cultures as Alternative Research Models. *Altern Lab Anim*. 2019;47(1):19-29. doi:10.1177/0261192919840092

585 12. Schaeffer J, Delpech C, Albert F, Belin S, Nawabi H. Adult Mouse Retina Explants: From ex
586 vivo to in vivo Model of Central Nervous System Injuries. *Front Mol Neurosci*.
587 2020;13:599948. doi:10.3389/fnmol.2020.599948

588 13. Hong Yee C, Aoki S, Uchihashi K, et al. The Air Liquid-interface, a Skin Microenvironment,
589 Promotes Growth of Melanoma Cells, but not Their Apoptosis and Invasion, through
590 Activation of Mitogen-activated Protein Kinase. *Acta Histochem Cytochem*. 2010;43(1):1-7.
591 doi:10.1267/ahc.09036

592 14. Jiang D, Schaefer N, Chu HW. Air–Liquid Interface Culture of Human and Mouse Airway
593 Epithelial Cells. In: Alper S, Janssen WJ, eds. *Lung Innate Immunity and Inflammation:*
594 *Methods and Protocols*. Methods in Molecular Biology. Springer; 2018:91-109.
595 doi:10.1007/978-1-4939-8570-8_8

596 15. Venkatesh A, Ma S, Langellotto F, Gao G, Punzo C. Retinal gene delivery by rAAV and DNA
597 electroporation. *Curr Protoc Microbiol*. 2013;0 14:Unit-14D.4.
598 doi:10.1002/9780471729259.mc14d04s28

599 16. Ail D, Malki H, Zin EA, Dalkara D. Adeno-Associated Virus (AAV) - Based Gene Therapies for
600 Retinal Diseases: Where are We? *Appl Clin Genet*. 2023;16:111-130.
601 doi:10.2147/TACG.S383453

602 17. Jeon CJ, Strettoi E, Masland RH. The Major Cell Populations of the Mouse Retina. *J Neurosci*.
603 1998;18(21):8936-8946. doi:10.1523/JNEUROSCI.18-21-08936.1998

604 18. Mahabadi N, Khalili YA. Neuroanatomy, Retina. In: *StatPearls [Internet]*. StatPearls
605 Publishing; 2023. Accessed December 3, 2023.
606 https://www.ncbi.nlm.nih.gov/books/NBK545310/

607 19. Kato M, Sudou N, Nomura-Komoike K, Iida T, Fujieda H. Age- and cell cycle-related
608 expression patterns of transcription factors and cell cycle regulators in Müller glia. *Sci Rep*.
609 2022;12(1):19584. doi:10.1038/s41598-022-23855-w

610 20. Pellissier LP, Hoek RM, Vos RM, et al. Specific tools for targeting and expression in Müller
611 glial cells. *Mol Ther - Methods Clin Dev*. 2014;1. doi:10.1038/mtm.2014.9

612 21. Poché RA, Furuta Y, Chaboissier MC, Schedl A, Behringer RR. Sox9 Is Expressed in Mouse
613 Multipotent Retinal Progenitor Cells and Functions in Müller Glial Cell Development. *J Comp*
614 *Neurol*. 2008;510(3):237-250. doi:10.1002/cne.21746

615 22. Feng G, Mellor RH, Bernstein M, et al. Imaging neuronal subsets in transgenic mice
616 expressing multiple spectral variants of GFP. *Neuron*. 2000;28(1):41-51. doi:10.1016/s0896-
617 6273(00)00084-2

618 23. Vazquez-Chona FR, Clark AM, Levine EM. *Rlbp1* Promoter Drives Robust Müller Glial GFP
619 Expression in Transgenic Mice. *Investig Opthalmology Vis Sci*. 2009;50(8):3996.
620 doi:10.1167/iovs.08-3189

621 24. Wang J, O'Sullivan ML, Mukherjee D, Puñal VM, Farsiu S, Kay JN. Anatomy and spatial
622 organization of Müller glia in mouse retina. *J Comp Neurol*. 2017;525(8):1759-1777.
623 doi:10.1002/cne.24153

624 25. Rashid K, Akhtar-Schaefer I, Langmann T. Microglia in Retinal Degeneration. *Front Immunol*.
625 2019;10:1975. doi:10.3389/fimmu.2019.01975

626 26. Wohl SG, Schmeer CW, Witte OW, Isenmann S. Proliferative Response of Microglia and
627 Macrophages in the Adult Mouse Eye after Optic Nerve Lesion. *Investig Opthalmology Vis*
628 *Sci*. 2010;51(5):2686. doi:10.1167/iovs.09-4537

629 27. Vázquez-Chona FR, Swan A, Ferrell WD, et al. Proliferative reactive gliosis is compatible with
630 glial metabolic support and neuronal function. *BMC Neurosci*. 2011;12(1):98.
631 doi:10.1186/1471-2202-12-98

632 28. Nomura-Komoike K, Saitoh F, Komoike Y, Fujieda H. DNA Damage Response in Proliferating
633 Müller Glia in the Mammalian Retina. *Investig Opthalmology Vis Sci*. 2016;57(3):1169.
634 doi:10.1167/iovs.15-18101

635 29. Goldman D. Müller glia cell reprogramming and retina regeneration. *Nat Rev Neurosci*.
636 2014;15(7):431-442. doi:10.1038/nrn3723

637 30. Hoang T, Wang J, Boyd P, et al. Gene regulatory networks controlling vertebrate retinal
638 regeneration. *Science*. 2020;370(6519):eabb8598. doi:10.1126/science.abb8598

639 31. Chen C, Bai X, Ding Y, Lee IS. Electrical stimulation as a novel tool for regulating cell
640 behavior in tissue engineering. *Biomater Res*. 2019;23:25. doi:10.1186/s40824-019-0176-8

641 32. Hernández-Bule ML, Paíno CL, Trillo MÁ, Úbeda A. Electric Stimulation at 448 kHz Promotes
642 Proliferation of Human Mesenchymal Stem Cells. *Cell Physiol Biochem*. 2014;34(5):1741-
643 1755. doi:10.1159/000366375

644 33. Katoh K. Effects of Electrical Stimulation of the Cell: Wound Healing, Cell Proliferation,
645 Apoptosis, and Signal Transduction. *Med Sci*. 2023;11(1):11. doi:10.3390/medsci11010011

646 34. Liu M, Xie D, Zeng H, Zhai N, Liu L, Yan H. Direct-current electric field stimulation promotes
647 proliferation and maintains stemness of mesenchymal stem cells. *BioTechniques*.
648 2023;74(6):293-301. doi:10.2144/btn-2022-0112

649 35. Martín D, Bocio-Nuñez J, Scagliusi SF, et al. DC electrical stimulation enhances proliferation
650 and differentiation on N2a and MC3T3 cell lines. *J Biol Eng*. 2022;16(1):27.
651 doi:10.1186/s13036-022-00306-8

652 36. Jullien N. Regulation of Cre recombinase by ligand-induced complementation of inactive
653 fragments. *Nucleic Acids Res*. 2003;31(21):131e-1131. doi:10.1093/nar/gng131

654 37. Tian X, Zhou B. Strategies for site-specific recombination with high efficiency and precise
655 spatiotemporal resolution. *J Biol Chem*. 2021;296:100509. doi:10.1016/j.jbc.2021.100509

656 38. Stachowski K, Norris AS, Potter D, Wysocki VH, Foster MP. Mechanisms of Cre recombinase
657 synaptic complex assembly and activation illuminated by Cryo-EM. *Nucleic Acids Res*.
658 2022;50(3):1753-1769. doi:10.1093/nar/gkac032

659 39. Stollmeier M, Kahlert S, Zuschratter W, et al. Air-liquid interface cultures trigger a metabolic
660 shift in intestinal epithelial cells (IPEC-1). *Histochem Cell Biol*. 2023;159(5):389-400.
661 doi:10.1007/s00418-023-02180-x

662 40. Gueven N, Glatthaar B, Manke HG, Haemmerle H. Co-cultivation of rat pneumocytes and
663 bovine endothelial cells on a liquid-air interface. *Eur Respir J*. 1996;9(5):968-975.
664 doi:10.1183/09031936.96.09050968

665 41. Vera MS, Simón MV, Prado Spalm FH, et al. Ceramide-1-phosphate promotes the migration
666 of retina Müller glial cells. *Exp Eye Res*. 2021;202:108359. doi:10.1016/j.exer.2020.108359

667 42. Goldman D. Müller glial cell reprogramming and retina regeneration. *Nat Rev Neurosci*.
668 2014;15(7):431-442. doi:10.1038/nrn3723

669 43. Tackenberg MA, Tucker BA, Swift JS, et al. Müller cell activation, proliferation and migration
670 following laser injury. *Mol Vis*. 2009;15:1886-1896.

671 44. Bringmann A, Iandiev I, Pannicke T, et al. Cellular signaling and factors involved in Müller
672 cell gliosis: Neuroprotective and detrimental effects. *Prog Retin Eye Res*. 2009;28(6):423-
673 451. doi:10.1016/j.preteyeres.2009.07.001

674 45. Nomura-Komoike K, Saitoh F, Fujieda H. Phosphatidylserine recognition and Rac1 activation
675 are required for Müller glia proliferation, gliosis and phagocytosis after retinal injury. *Sci*
676 *Rep*. 2020;10(1):1488. doi:10.1038/s41598-020-58424-6

677 46. Jones BW, Watt CB, Frederick JM, et al. Retinal remodeling triggered by photoreceptor
678 degenerations. *J Comp Neurol*. 2003;464(1):1-16. doi:10.1002/cne.10703

679 47. Kumar A, Nune K, Misra R. Understanding the response of pulsed electric field on osteoblast
680 functions in three-dimensional mesh structures. *J Biomater Appl*. 2016;31(4):594-605.
681 doi:10.1177/0885328216658376

682 48. Zhu W, Ye T, Lee SJ, et al. Enhanced neural stem cell functions in conductive annealed
683 carbon nanofibrous scaffolds with electrical stimulation. *Nanomedicine Nanotechnol Biol*
684 *Med*. 2018;14(7):2485-2494. doi:10.1016/j.nano.2017.03.018

685 49. Snyder S, DeJulius C, Willits RK. Electrical Stimulation Increases Random Migration of
686 Human Dermal Fibroblasts. *Ann Biomed Eng*. 2017;45(9):2049-2060. doi:10.1007/s10439-
687 017-1849-x

688 50. Zhao H, Steiger A, Nohner M, Ye H. Specific Intensity Direct Current (DC) Electric Field
689 Improves Neural Stem Cell Migration and Enhances Differentiation towards βIII-Tubulin+
690 Neurons. *PLoS ONE*. 2015;10(6):e0129625. doi:10.1371/journal.pone.0129625

691 51. Dong Z yong, Pei Z, Li Z, Wang Y ling, Khan A, Meng X ting. Electric field stimulation induced
692 neuronal differentiation of filum terminale derived neural progenitor cells. *Neurosci Lett*.
693 2017;651:109-115. doi:10.1016/j.neulet.2017.05.001

694 52. Ryan CNM, Doulgkeroglou MN, Zeugolis DI. Electric field stimulation for tissue engineering
695 applications. *BMC Biomed Eng*. 2021;3:1. doi:10.1186/s42490-020-00046-0

696

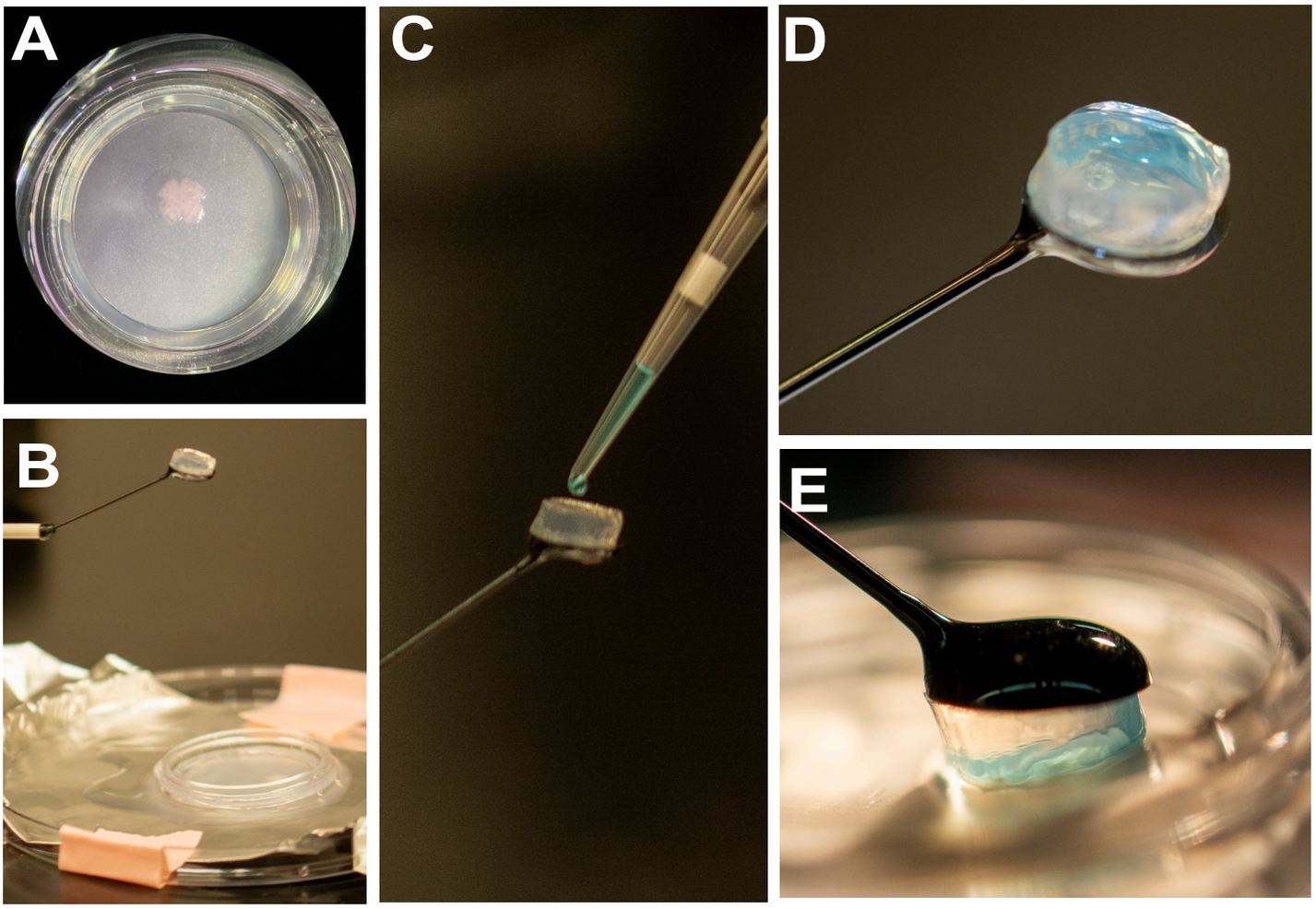
A
B
C
D
E

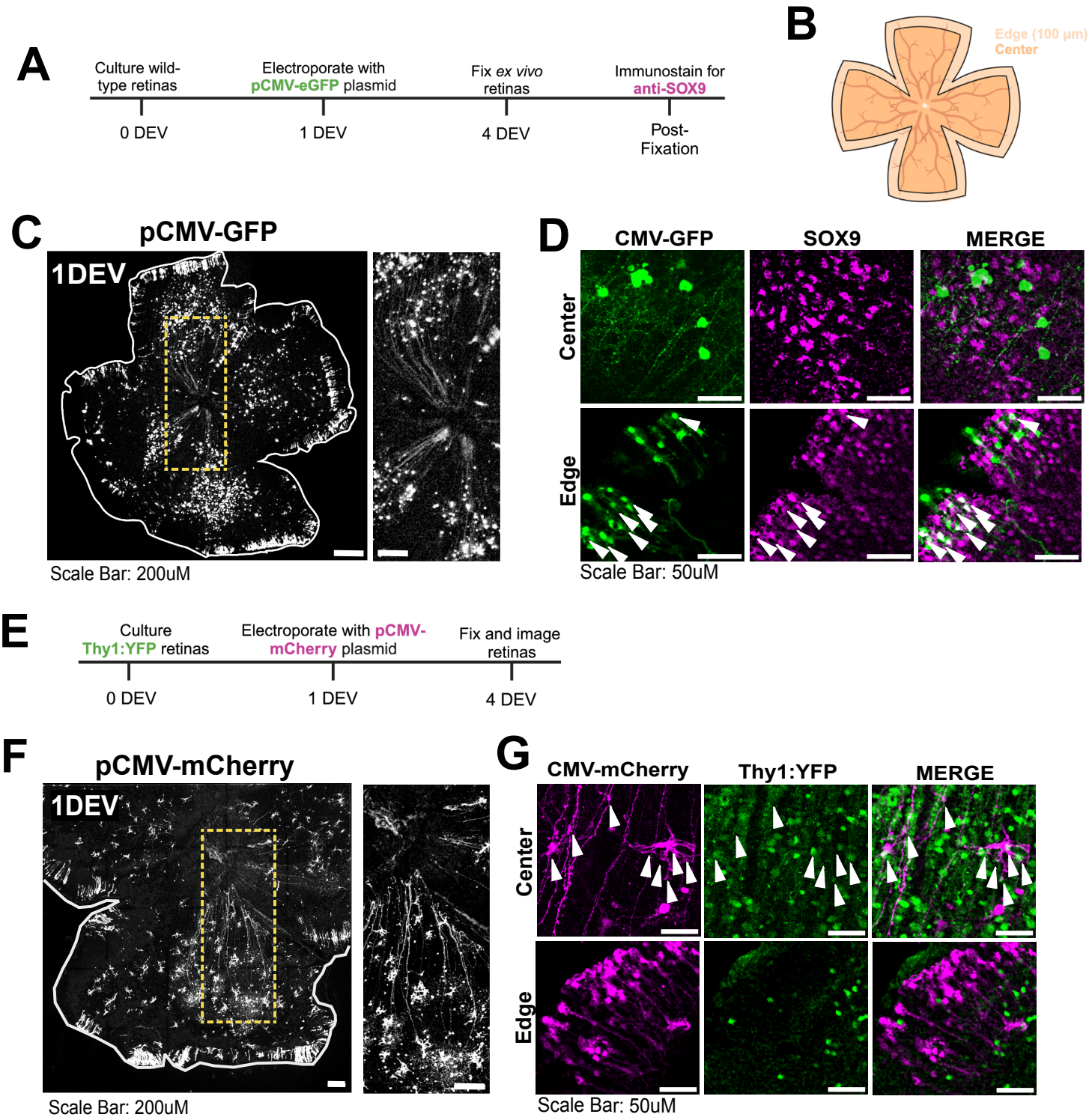
A
Culture wild-type retinas
Electroporate with pCMV-eGFP plasmid
Fix ex vivo retinas
Immunostain for anti-SOX9
0 DEV
1 DEV
4 DEV
Post-Fixation
B
Edge (100 µm)
Center
C
pCMV-GFP
1DEV
Scale Bar: 200uM
D
CMV-GFP
SOX9
MERGE
Center
Edge
Scale Bar: 50uM
E
Culture Thy1:YFP retinas
Electroporate with pCMV-mCherry plasmid
Fix and image retinas
0 DEV
1 DEV
4 DEV
F
pCMV-mCherry
1DEV
Scale Bar: 200uM
G
CMV-mCherry
Thy1:YFP
MERGE
Center
Edge
Scale Bar: 50uM
H
Cell types transfected at 1DEV
% Transfected Cells
1.0
0.8
0.6
0.4
0.2
0.0
***
****
****
****
**
**
Edge
Center
Edge & Center
Transfected Müller glia (Sox9+eGFP+/eGFP+)
Transfected neurons (Thy1:YFP+ mCherry+/mCherry+)

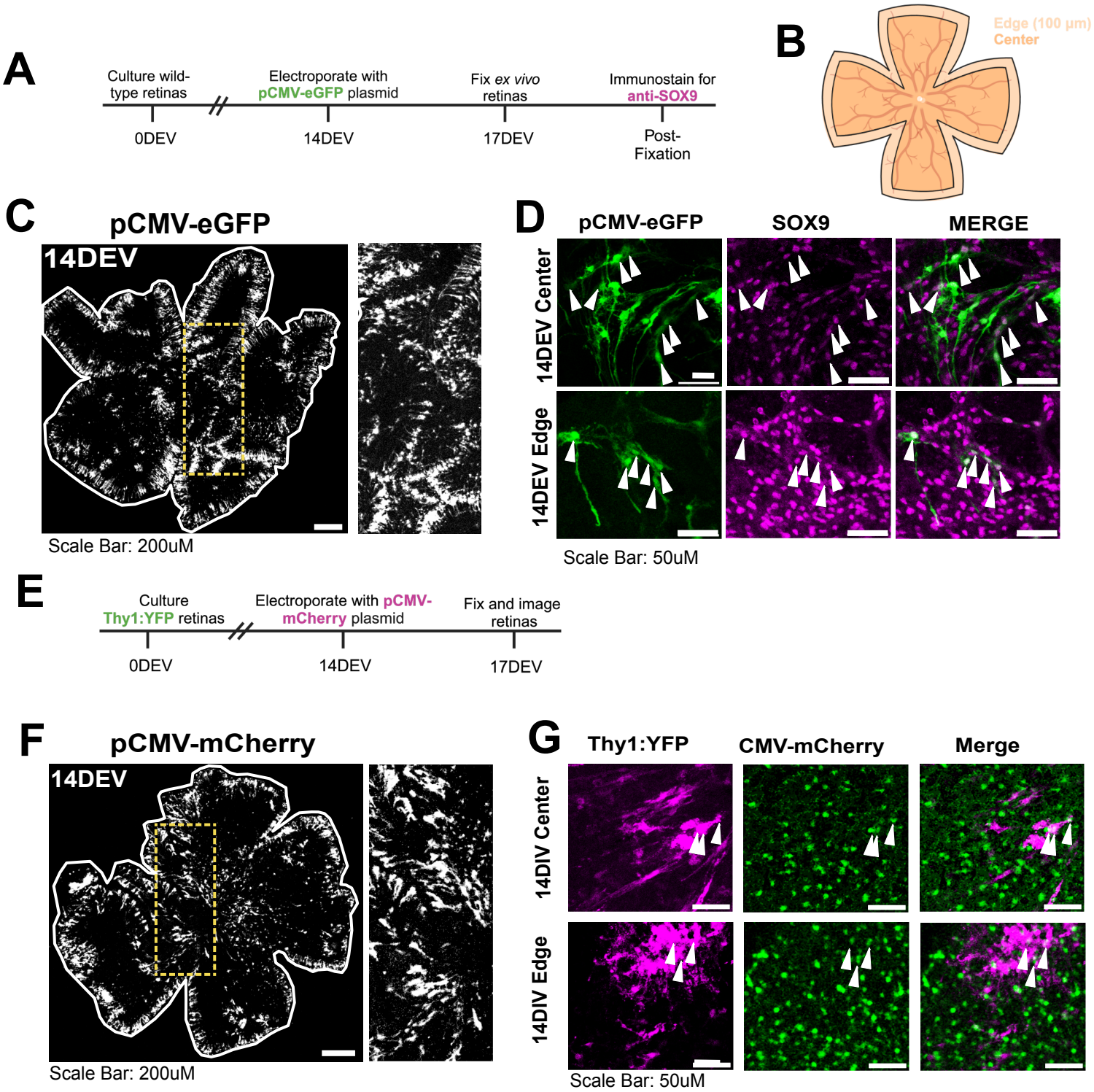
A
Culture wild-type retinas
Electroporate with pCMV-eGFP plasmid
Fix ex vivo retinas
Immunostain for anti-SOX9
0DEV
14DEV
17DEV
Post-Fixation
B
Edge (100 µm)
Center
C
pCMV-eGFP
14DEV
Scale Bar: 200uM
D
pCMV-eGFP
SOX9
MERGE
14DEV Center
14DEV Edge
Scale Bar: 50uM
E
Culture Thy1:YFP retinas
Electroporate with pCMV-mCherry plasmid
Fix and image retinas
0DEV
14DEV
17DEV
F
pCMV-mCherry
14DEV
Scale Bar: 200uM
G
Thy1:YFP
CMV-mCherry
Merge
14DIV Center
14DIV Edge
Scale Bar: 50uM
H
Cell types transfected at 14DEV
% Transfected Cells
1.0
0.8
0.6
0.4
0.2
0.0
****
****
****
Edge
Center
Edge & Center
Transfected Müller glia (Sox9+eGFP+/eGFP+)
Transfected neurons (Thy1:YFP+ mCherry+/mCherry+)

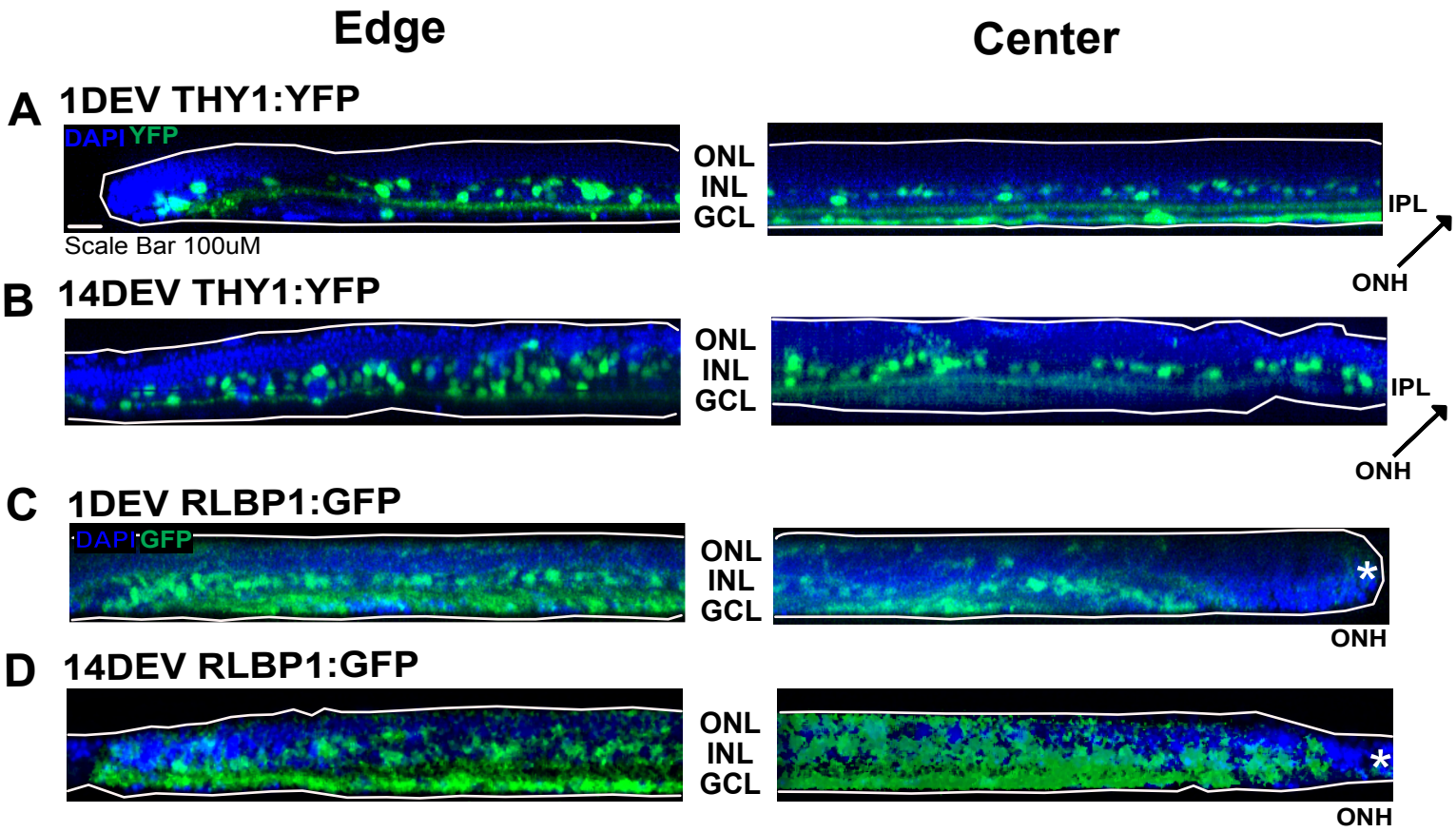
Edge
Center
A
1DEV THY1:YFP
DAPI YFP
Scale Bar 100uM
ONL
INL
GCL
IPL
ONH
B
14DEV THY1:YFP
ONL
INL
GCL
IPL
ONH
C
1DEV RLBP1:GFP
DAPI GFP
ONL
INL
GCL
*
ONH
D
14DEV RLBP1:GFP
ONL
INL
GCL
*
ONH

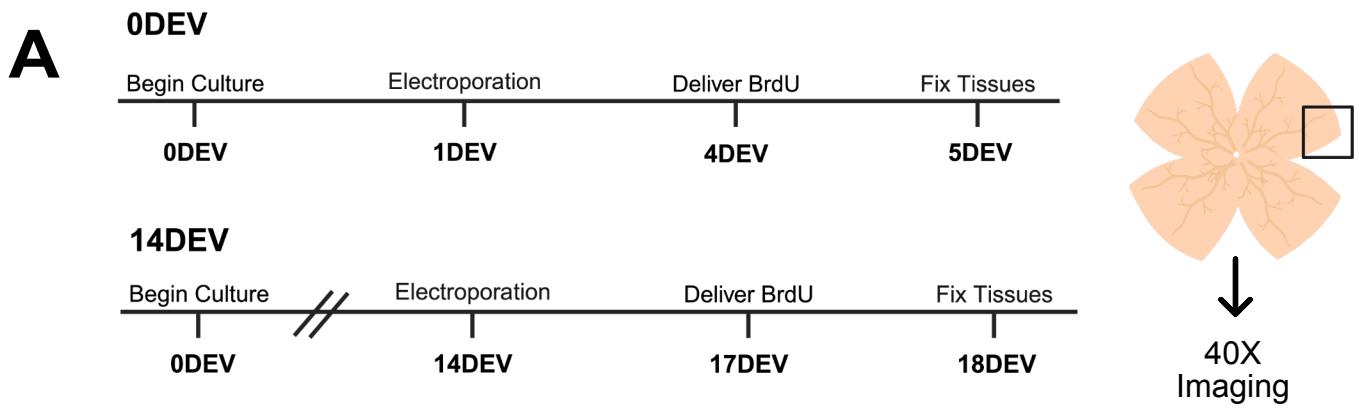
A
0DEV
Begin Culture
Electroporation
Deliver BrdU
Fix Tissues
0DEV
1DEV
4DEV
5DEV
14DEV
Begin Culture
Electroporation
Deliver BrdU
Fix Tissues
0DEV
14DEV
17DEV
18DEV
40X
Imaging

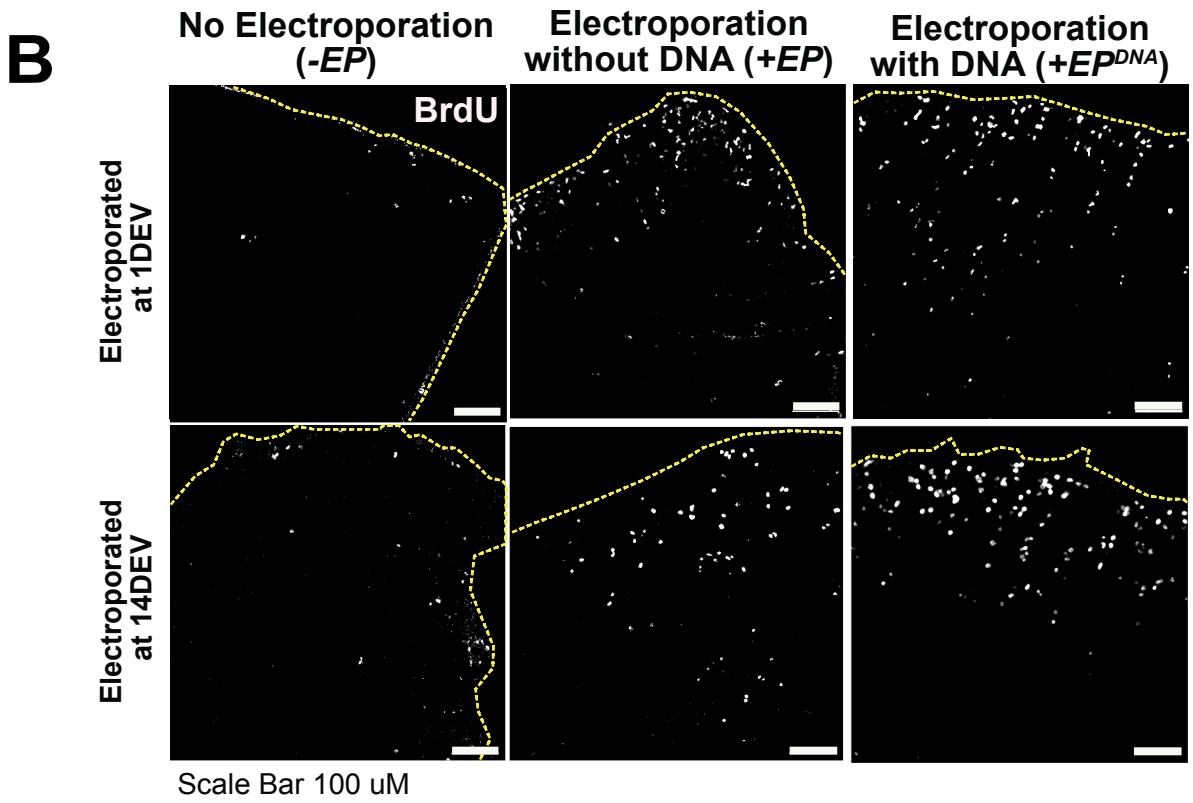
B
No Electroporation
(-EP)
Electroporation
without DNA (+EP)
Electroporation
with DNA (+EP^DNA)
BrdU
Electroporated
at 1DEV
Electroporated
at 14DEV
Scale Bar 100 uM

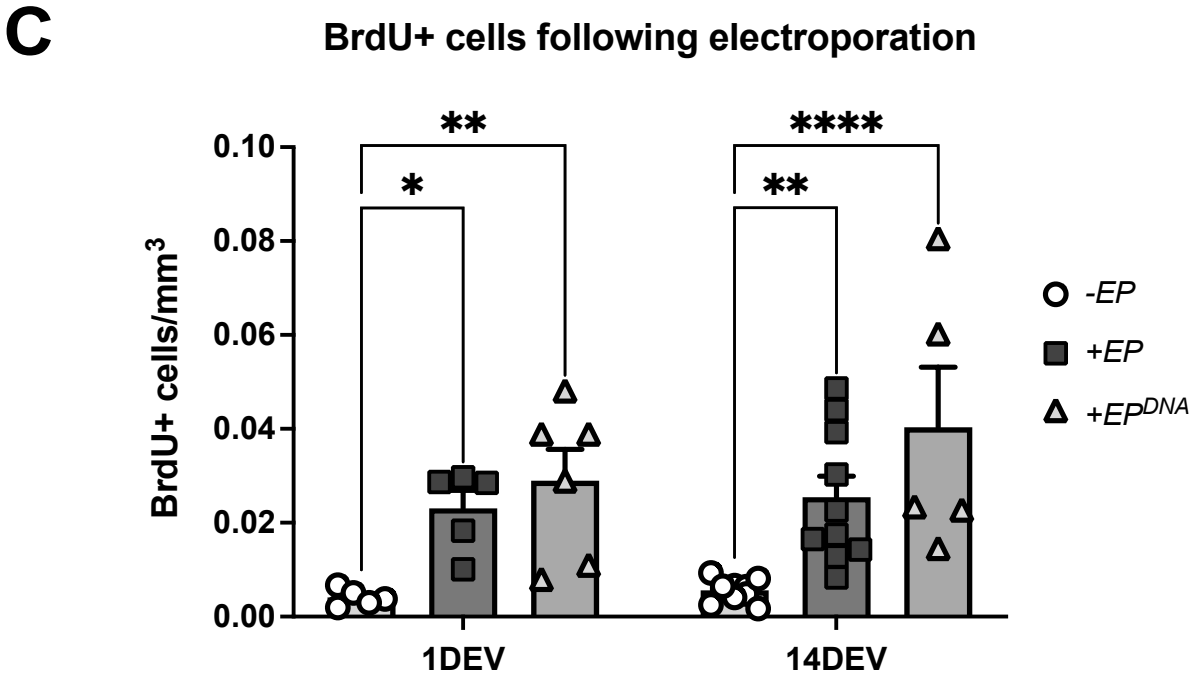
C
BrdU+ cells following electroporation
BrdU+ cells/mm3
0.10
0.08
0.06
0.04
0.02
0.00
**
*
****
**
1DEV
14DEV
-EP
+EP
+EP^DNA

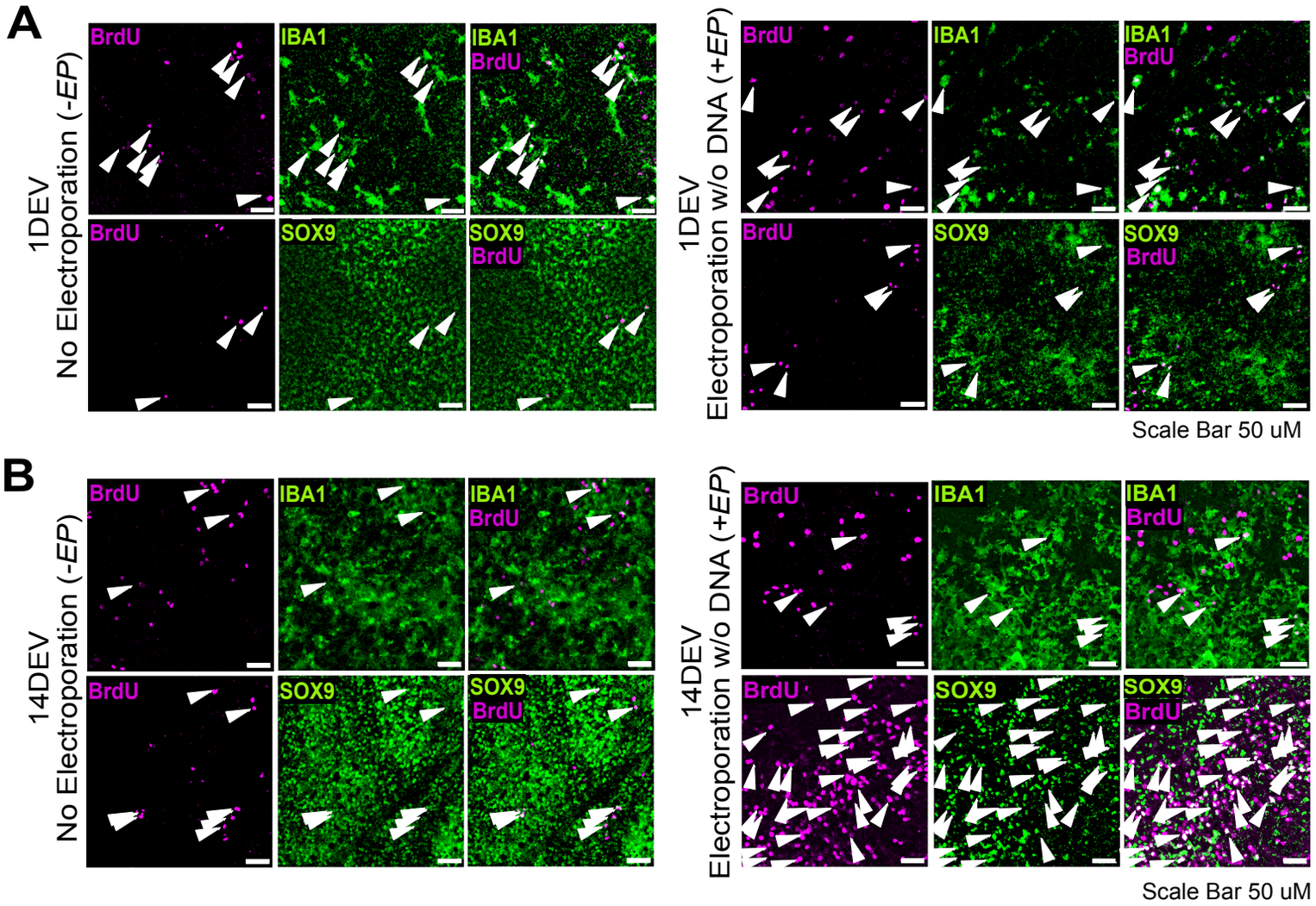
A
1DEV
No Electroporation (-EP)
1DEV
Electroporation w/o DNA (+EP)
BrdU
IBA1
IBA1
BrdU
SOX9
SOX9
BrdU
Scale Bar 50 uM
B
14DEV
No Electroporation (-EP)
14DEV
Electroporation w/o DNA (+EP)
Scale Bar 50 uM

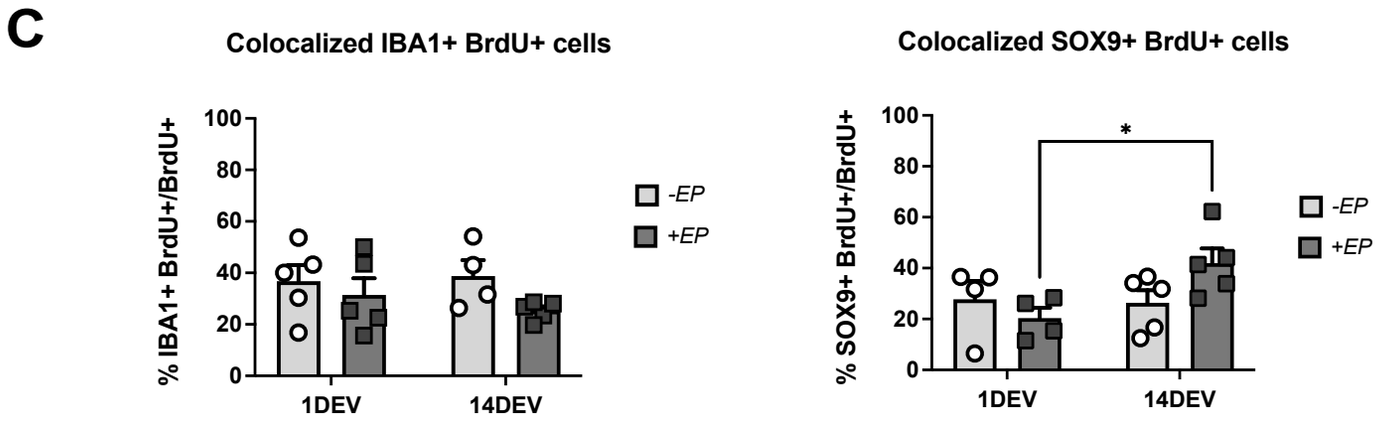
C
Colocalized IBA1+ BrdU+ cells
% IBA1+ BrdU+/BrdU+
100
80
60
40
20
0
1DEV
14DEV
-EP
+EP
Colocalized SOX9+ BrdU+ cells
% SOX9+ BrdU+/BrdU+
*

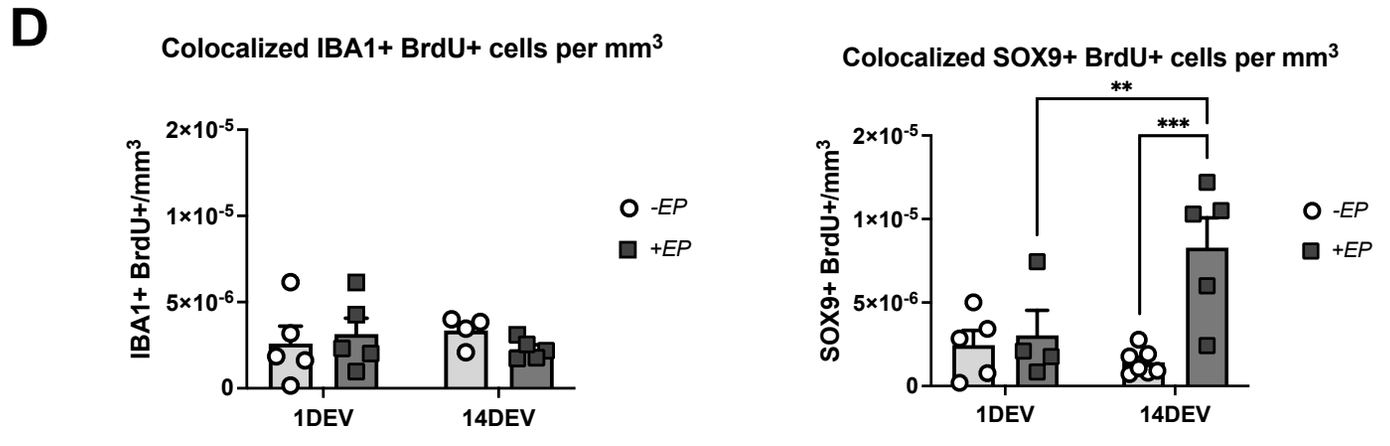
D
Colocalized IBA1+ BrdU+ cells per mm3
IBA1+ BrdU+/mm3
2×10-5
1×10-5
5×10-6
0
1DEV
14DEV
-EP
+EP
Colocalized SOX9+ BrdU+ cells per mm3
SOX9+ BrdU+/mm3
**
***

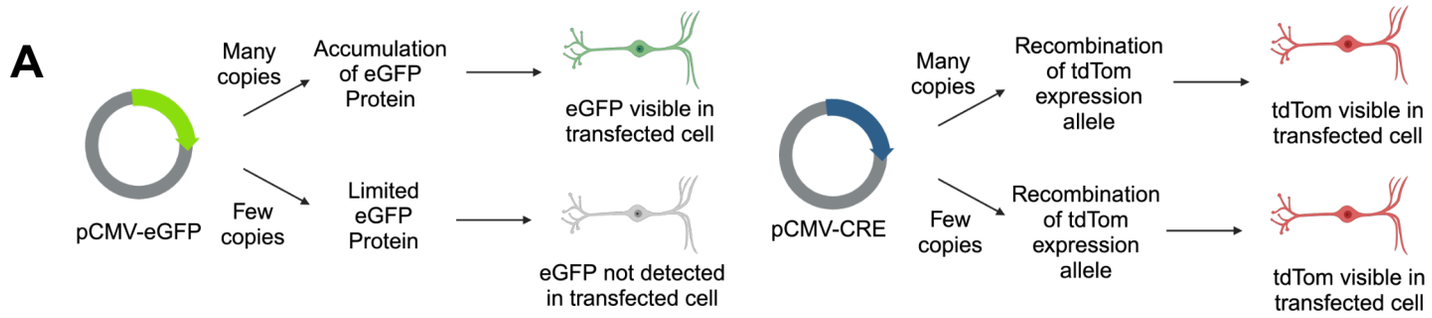
A
pCMV-eGFP
Many copies
Accumulation of eGFP Protein
eGFP visible in transfected cell
Few copies
Limited eGFP Protein
eGFP not detected in transfected cell
pCMV-CRE
Many copies
Recombination of tdTom expression allele
tdTom visible in transfected cell
Few copies
Recombination of tdTom expression allele
tdTom visible in transfected cell

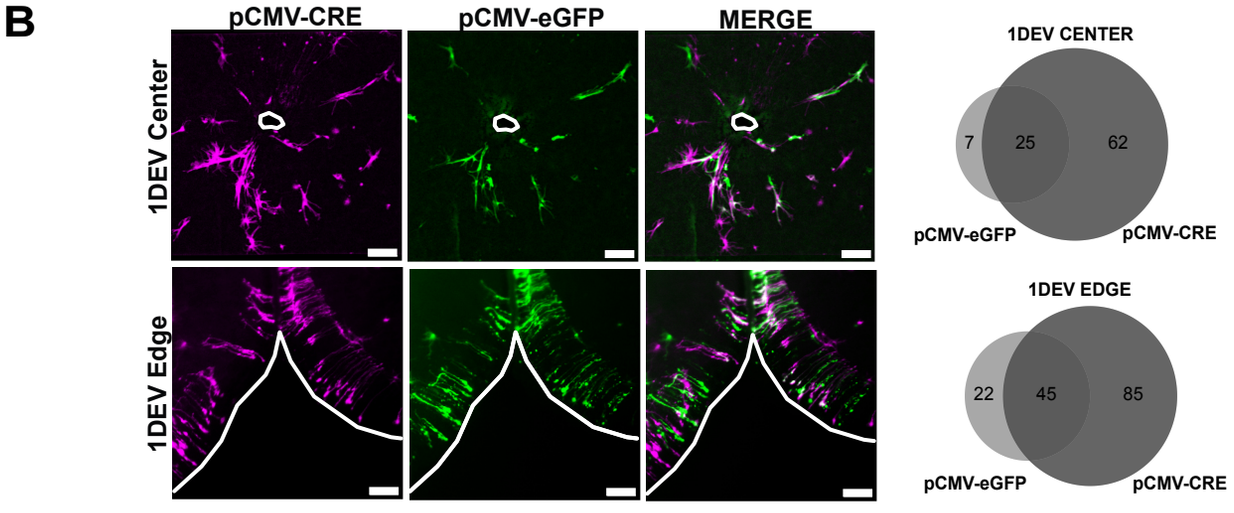
B
pCMV-CRE
pCMV-eGFP
MERGE
1DEV Center
1DEV Edge
1DEV CENTER
7
25
62
pCMV-eGFP
pCMV-CRE
1DEV EDGE
22
45
85
pCMV-eGFP
pCMV-CRE

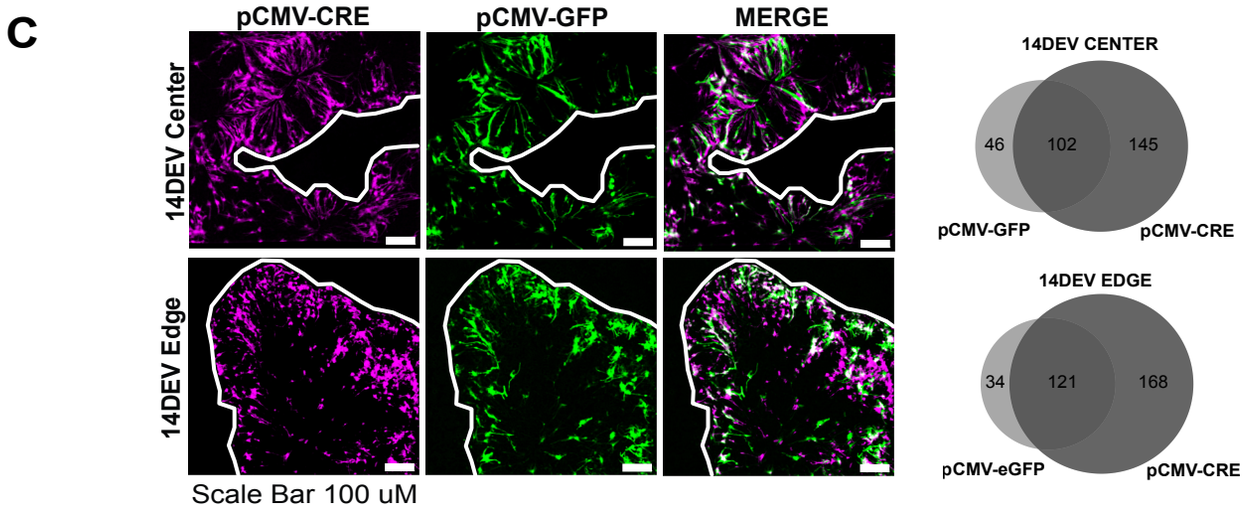
C
pCMV-CRE
pCMV-GFP
MERGE
14DEV Center
14DEV Edge
14DEV CENTER
46
102
145
pCMV-GFP
pCMV-CRE
14DEV EDGE
34
121
168
pCMV-eGFP
pCMV-CRE
Scale Bar 100 uM

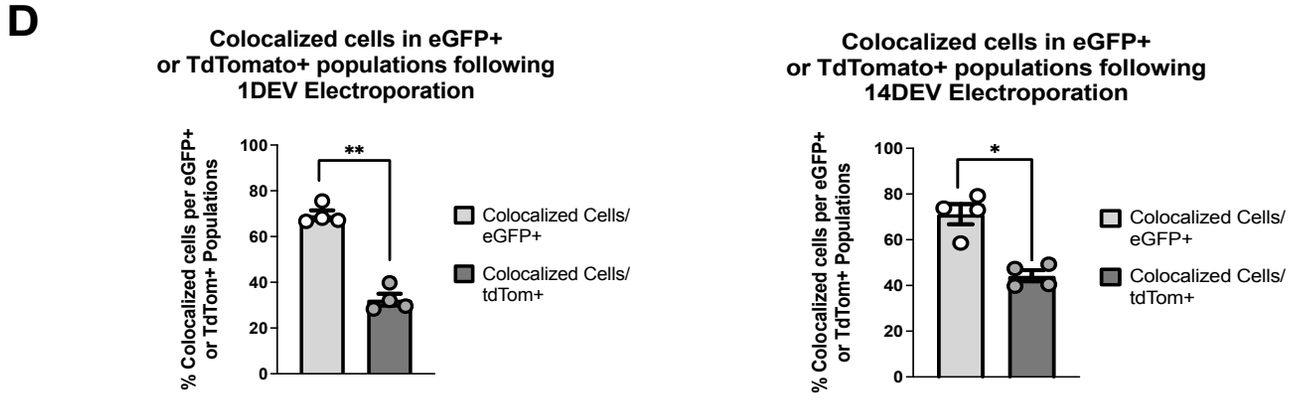
D
Colocalized cells in eGFP+ or TdTomato+ populations following 1DEV Electroporation
% Colocalized cells per eGFP+ or TdTom+ Populations
100
80
60
40
20
0
**
Colocalized Cells/ eGFP+
Colocalized Cells/ tdTom+
Colocalized cells in eGFP+ or TdTomato+ populations following 14DEV Electroporation
% Colocalized cells per eGFP+ or TdTom+ Populations
100
80
60
40
20
0
*
Colocalized Cells/ eGFP+
Colocalized Cells/ tdTom+

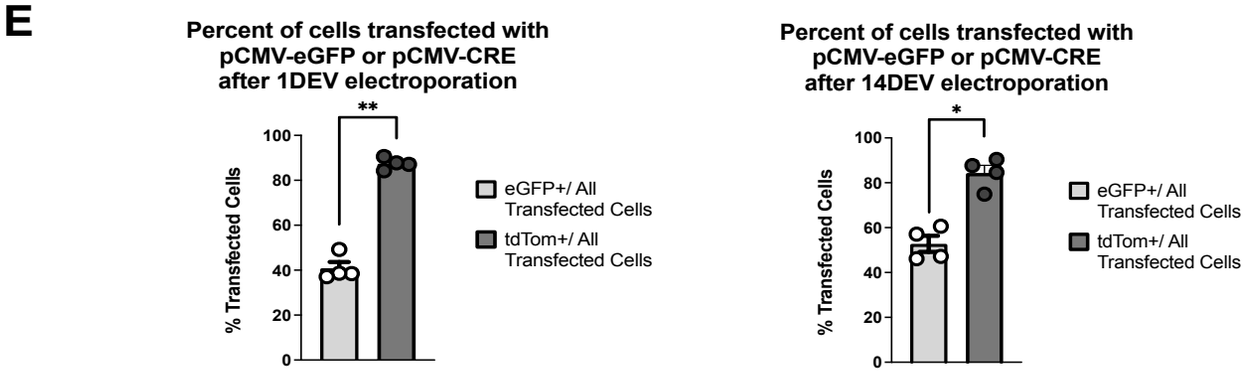
E
Percent of cells transfected with pCMV-eGFP or pCMV-CRE after 1DEV electroporation
% Transfected Cells
100
80
60
40
20
0
**
eGFP+/ All Transfected Cells
tdTom+/ All Transfected Cells
Percent of cells transfected with pCMV-eGFP or pCMV-CRE after 14DEV electroporation
% Transfected Cells
100
80
60
40
20
0
*
eGFP+/ All Transfected Cells
tdTom+/ All Transfected Cells